Radiology

Lung Adenocarcinoma: Correlation of Quantitative CT Findings with Pathologic Findings[1]

Jane P. Ko, MD
James Suh, MD
Opeyemi Ibidapo, MD
Joanna G. Escalon, MD
Jinyu Li, MA
Harvey Pass, MD
David P. Naidich, MD
Bernard Crawford, MD
Emily B. Tsai, MD[2]
Chi Wan Koo, MD[3]
Artem Mikheev, BS
Henry Rusinek, PhD

Purpose: To identify the ability of computer-derived three-dimensional (3D) computed tomographic (CT) segmentation techniques to help differentiate lung adenocarcinoma subtypes.

Materials and Methods: This study had institutional research board approval and was HIPAA compliant. Pathologically classified resected lung adenocarcinomas (n = 23) with thin-section CT data were identified. Two readers independently placed over-inclusive volumes around nodules from which automated computer measurements were generated: mass (total mass) and volume (total volume) of the nodule and of any solid portion, in addition to the solid percentage of the nodule volume (percentage solid volume) or mass (percentage solid mass). Interobserver agreement and differences in measurements among pathologic entities were evaluated by using t tests. A multinomial logistic regression model was used to differentiate the probability of three diagnoses: invasive non–lepidic-predominant adenocarcinoma (INV), lepidic-predominant adenocarcinoma (LPA), and adenocarcinoma in situ (AIS)/minimally invasive adenocarcinoma (MIA).

Results: Mean percentage solid volume of INV was 35.4% (95% confidence interval [CI]: 26.2%, 44.5%)—higher than the 14.5% (95% CI: 10.3%, 18.7%) for LPA (P = .002). Mean percentage solid volume of AIS/MIA was 8.2% (95% CI: 2.7%, 13.7%) and had a trend toward being lower than that for LPA (P = .051). Accuracy of the model based on total volume and percentage solid volume was 73.2%; accuracy of the model based on total mass and percentage solid mass was 75.6%.

Conclusion: Computer-assisted 3D measurement of nodules at CT had good reproducibility and helped differentiate among subtypes of lung adenocarcinoma.

[1] From the Departments of Radiology (J.P.K., O.I., J.G.E., J.L., D.P.N., E.B.T., C.W.K., A.M., H.R.), Pathology (J.S.), and Cardiothoracic Surgery (H.P., B.C.), New York University School of Medicine, NYU Langone Medical Center, 660 First Ave, 7th Floor, New York, NY 10016; and Department of Radiology, New York-Presbyterian Hospital-Weill Cornell Medical Center, New York, NY (J.G.E.). Received January 14, 2015; revision requested March 16; revision received December 18; accepted January 7, 2016; final version accepted January 20. **Address correspondence to** J.P.K. (e-mail: *jane.ko@nyumc.org*).

[2] **Current address:** Department of Radiological Sciences, David Geffen School of Medicine at UCLA, Los Angeles, Calif.

[3] **Current address:** Department of Radiology, Mayo Clinic, Rochester, Minn.

Subsolid nodules are challenging, given their poorly defined margins, heterogeneous internal features, and varying attenuations, and their evaluation may benefit particularly from computer-assisted techniques. Currently, the assessment of the degree of solid components within subsolid nodules is typically performed by using the maximal dimensions of the soft-tissue component (1,2). Other quantitative measures, such as the tumor disappearance rate, that are primarily determined by using two-dimensional caliper measurements, have been investigated, although they are are not widely implemented in clinical practice (3,4). Additionally, the measurement of nodule volume has been reported to show better measurement precision and accuracy than maximal dimensions, although this has been investigated to a lesser degree for subsolid nodules (5,6). More recently, three-dimensional (3D) volumetric assessment of the volume and mass of subsolid nodules with segmentation techniques is receiving increasing attention (7–10).

Subsolid nodules are associated with lung adenocarcinoma (1,7,11–15), whose classification was recently revised by the International Association for the Study of Lung Cancer (IASLC)/American Thoracic Society (ATS)/European Respiratory Society (ERS) (16) to provide uniform terminology, more specific diagnostic criteria, and better stratification of constituents. The degree of predominant histologic finding is used to render the diagnosis, with use of the terms adenocarcinoma in situ (AIS), minimally invasive carcinoma (MIA), and lepidic-predominant adenocarcinoma (LPA) for adenocarcinomas containing mainly lepidic or noninvasive growth (16). The diagnoses of "bronchioloalveolar" (or bronchoalveolar) carcinoma (17,18) have been eliminated.

Our objective was to identify the ability of computer-derived 3D computed tomography (CT) segmentation techniques to help differentiate lung adenocarcinoma subtypes.

Advances in Knowledge

- The percentage solid volume and the percentage of solid mass in relation to the mass of the entire nodule (percentage solid mass) increases with more aggressive adenocarcinoma histopathology, as classified by the IASLC/ATS/ERS; percentage solid volume was 8.2% ± 6.5 for adenocarcinoma in situ (AIS), 14.5% ± 6.6 for lepidic-predominant adenocarcinoma (LPA), and 35.4% ± 20.2 for other invasive non–lepidic-predominant carcinomas (INVs), while percentage solid mass was 14.2% ± 10.6 for AIS, 23.0% ± 8.8 for LPA, and 46.6% ± 21.2 for INV.
- The percentage solid volume (P = .002) and percentage solid mass (P = .001) differed between LPA and INV; the mass of the entire nodule and the volume of any solid portion differed for LPA and minimally invasive carcinoma/AIS but not for LPA and INV.
- Automated analysis of CT images can be used to differentiate adenocarcinoma subtypes; three categories were differentiated with an overall accuracy of 73.2% by using multivariate models of percentage solid volume, and the accuracy was 75.6% for discrimination based on percentage solid mass and total nodule mass.
- A computer-assisted method is highly reproducible, with intraclass correlation coefficients of 0.996 (95% CI: 0.991, 0.998) for solid volume and 0.986 (95% CI: 0.954, 0.996) for solid portion of the nodule (percentage solid volume).

Implication for Patient Care

- Further understanding of the correlation of quantitative three-dimensional CT measures with IASLC/ATR/ERS histologic classifications may enable noninvasive characterization of suspected primary lung adenocarcinoma; such ability could aid in decisions as to whether lung resection is undertaken in contrast to more conservative follow-up of patients to avoid overtreatment.

Materials and Methods

Patients and Chest CT Data

This study was approved by the Institutional Research Board with a waiver of consent and was Health Insurance Portability and Accountability Act compliant. From a thoracic lung cancer database of 138 patients with resected and pathologically confirmed stage I adenocarcinomas between September 19, 2006, and September 29, 2014, for whom a tissue microarray had been constructed, we identified and retrieved the chest CT studies performed at our institution of all patients who had thin-section (1-mm) images. Chest CT studies had been performed on multidetector CT scanners with a 64– (Definition) or 128–detector row configuration

Published online before print
10.1148/radiol.2016142975 **Content codes:** CH CT

Radiology 2016; 000:1–9

Abbreviations:
AIS = adenocarcinoma in situ
ATS = American Thoracic Society
CI = confidence interval
ERS = European Respiratory Society
IASLC = International Association for the Study of Lung Cancer
INV = invasive non–lepidic-predominant carcinoma
LPA = lepidic-predominant adenocarcinoma
MIA = minimally invasive carcinoma
3D = three-dimensional
VOI = volume of interest

Author contributions:
Guarantors of integrity of entire study, J.P.K., O.I.; study concepts/study design or data acquisition or data analysis/interpretation, all authors; manuscript drafting or manuscript revision for important intellectual content, all authors; manuscript final version approval, all authors; agrees to ensure any questions related to the work are appropriately resolved, all authors; literature research, J.P.K., O.I., E.B.T., H.R.; clinical studies, J.P.K., J.S., J.L., H.P., D.P.N., B.C.; experimental studies, J.S., J.L., A.M., H.R.; statistical analysis, O.I., E.B.T., H.R.; and manuscript editing, J.P.K., J.S., O.I., J.G.E., J.L., H.P., D.P.N., C.W.K., H.R.

Conflicts of interest are listed at the end of this article.

(Definition AS+ or Definition Flash; Siemens, Malvern, Pa). The protocol included the following parameters: reference 80–160 mAs tube current time, 120 kVp, gantry rotation time of 0.33–0.50 second, and tube current modulation. CT images were reconstructed with a high-frequency (b60) reconstruction kernel into a 512 × 512 matrix and field of view to contain the patient's lungs. Thin-section images were 1.0-mm sections reconstructed at 0.8-mm intervals.

For the correlation of histopathologic findings with CT quantitative measures, the imaging examination that was closest to the date of tumor resection was used for analysis. Studies of 42 patients were excluded if thin-section CT studies were not performed within 90 days prior to the date of surgical resection or if CT involved intravenous administration of contrast material. Thus, a cohort of 41 noncontrast thin-section CT studies in 41 patients with stage I lung adenocarcinoma were analyzed and were correlated with histopathologic findings. Of the 41 patients, 11 were men (mean age, 73 years ± 7.6 [standard deviation]; range, 54–81 years) and 30 were women (mean age, 70 years ± 7.0; range, 47–82 years) (independent samples *t* test, $t = 2.11$, $P = .30$). The mean age of the entire cohort was 70.6 years ± 7.2 (range, 47–82 years). The CT study closest to resection had been performed a mean of 39.5 days ± 21.1 prior to surgical resection.

A pulmonary pathologist with 1–2 years of experience (J.S.) who was unaware of the imaging findings had evaluated and classified the adenocarcinomas according to the newly introduced IASLC/ATS/ERS international multidisciplinary classification (16). The predominant cell type was determined, in addition to the percentage of this predominant cell type. The specimens were categorized as atypical adenomatous hyperplasia, AIS, MIA, LPA, papillary, acinar, micropapillary, solid, and other adenocarcinoma histologic findings. The invasive subtypes other than LPA were considered as one group of invasive nonlepidic-predominant adenocarcinomas (INVs). Acinar and papillary histologic subtypes, given their intermediate-grade patterns of invasion, and micropapillary and solid tumors, considered to have high-grade patterns of invasion, were grouped together for analysis.

CT data prior to analysis were assigned anonymous identifiers. A thoracic radiologist with 17 years of postfellowship experience (J.P.K.) who was blinded to the pathologic results visually evaluated features of nodules. Nodule margin was classified as smooth, lobulated, or irregular (19). Nodule shape was categorized as round, oval, or amorphous (19). Amorphous nodules were those nodules that were not characterized as round or oval. Pseudocavitation was defined as small rounded bubble lucencies within the nodule (14,19). Pleural tag, defined as a linear density extending from the nodule to the pleura, was evaluated (14,19). Internal reticulation was considered to be present when a reticular network of intralobular lines was visualized within a nodule (20). Nodule location was characterized as either central (within the inner two-thirds of a lobe) or peripheral (within the outer third of a lobe) (21).

Automated 3D Nodule Volume Measurement

Each subsolid nodule was segmented by extending a previously described method (22) and using a locally developed software program. After a training session of five cases, a radiology resident (O.I.) and a 4th-year medical student (J.G.E.) blinded to the pathologic diagnosis independently placed overinclusive volumes of interest (VOIs) around 19 lung nodules on each section in which the nodule was visualized (Fig 1, red region). A thoracic radiologist with 30 years of experience (D.P.N.) and the radiology resident each segmented 12 additional nodules, while a thoracic radiologist with 17 years of postfellowship experience (J.P.K.) segmented 10 more cases using the same process.

The VOI encompassed the nodule and included a rim of approximately 1–3 mm of surrounding lung. The reader excluded any blood vessels and the chest wall abutting the margin of the nodule. VOI delineation took 35 seconds, on average. The program then automatically normalized the rim size, estimated the distribution of lung background attenuation by averaging the attenuation of all voxels located along the edge of the region that were below −700 HU, and constructed the subsolid nodule mask (Fig 1, yellow region).

The solid component was defined by using the threshold of −188 HU. This value was based on a 95% distribution of manually segmented solid component (see below). To calculate the mass, the program converted for each voxel i its attenuation a_i, expressed in Hounsfield units, to the density (specific gravity), expressed in grams per milliliter, with the following equation: $d_i = (a_i + 1000)/1000$.

The equation derives from air having attenuation of −1000 HU and negligible mass (9). For example, a voxel with attenuation 0 HU (water) will have a density of 1 g/mL. The mass is computed as the product of voxel volume by its density d_i and summed over the nodule mask. The solid component is computed separately (Fig 2). We then computed *(a)* the volume of the solid component as the fraction of nodule volume, expressed as a percentage (percentage solid volume), and *(b)* the mass and the fraction of nodule mass that the solid component represented (percentage solid mass).

Statistical Analysis

t Tests were used to compare each imaging measure among AIS and MIA, LPA, and INV. $P < .05$ was considered to indicate a significant difference. A multinomial logistic regression model was used to identify probabilities of three different outcomes: INV, LPA, and AIS/MIA. MIA and AIS were combined in the analysis given their similar survival rates. Multinomial regression is similar to logistic regression but can, however, handle more than two outcomes. Model parameters were estimated through an iterative maximum-likelihood algorithm. Three separate regression models were constructed for different choices of CT measures. χ^2 Analysis was used to analyze the goodness of fit. The Akaike information criterion was used as a measure of the relative quality of a model that includes a penalty for increasing the number of free variables

Figure 1

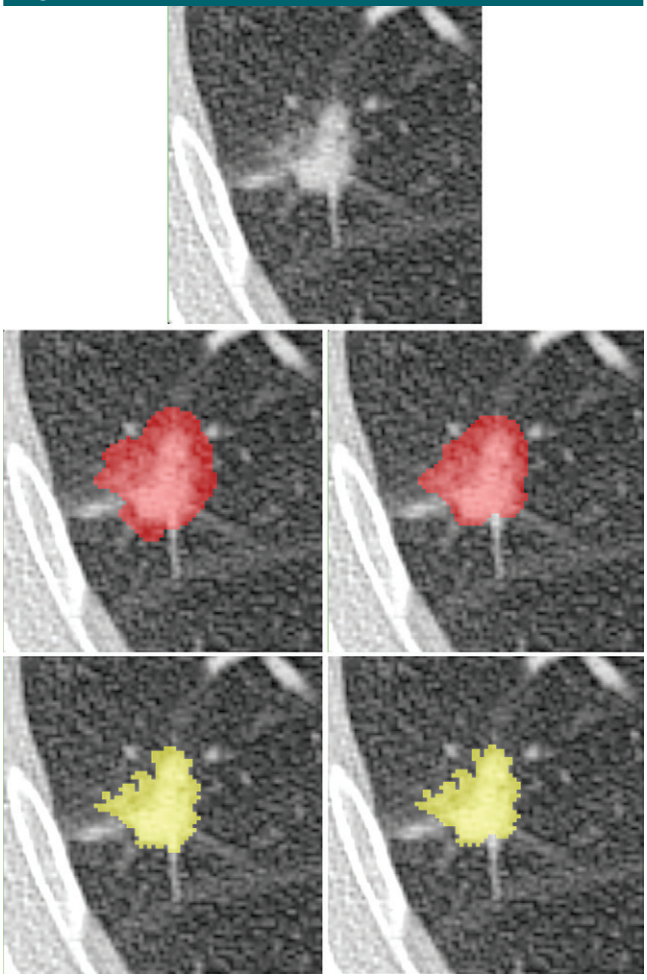

Figure 1: Automated segmentation of subsolid nodule. Top: CT image of the nodule. Middle row: Masks generated by two observers. Bottom row: The final nodule masks (yellow) are derived from the initial overinclusive masks (middle row) by the algorithm. Note that the final masks are similar in spite of the differences in the initial regions.

to discourage overfitting. Interobserver agreement on all measures was assessed by using interclass correlation coefficients. Statistical analysis was performed by using SPSS software (version 23; IBM, Armonk, NY).

Results

Pathologic diagnoses of the adenocarcinomas were 21 INVs, 12 LPAs, five MIAs, and three AISs. Table 1 describes imaging measures across diagnostic subgroups. No significant difference between LPA and INV was identified for total volume or total mass. In distinction, percentage solid volume was significantly higher for INV than for LPA (P = .002), and a trend (P = .051) distinguished LPA compared with AIS and MIA combined (Table 1). Specifically, percentage solid volume averaged 35.4% ± 20.2 (95% CI: 26.2%, 44.5%) for INV, 14.5% ± 6.6 (95% CI: 10.3%, 18.7%) for LPA, and 8.2% ± 6.5 (95% CI: 2.7%, 13.7%) for AIS and MIA in combination. Similarly, percentage solid mass differentiated between INV and LPA (P = .001) (Table 1).

Total solid volume did not significantly differ between INV, with 3558 mm^3 ± 3681 (95% CI: 1883, 5234) and LPA, with 4171 mm^3 ± 3798 (95% CI: 1822, 6521) ($P > .05$), but a significant difference (P = .041) was identified between LPA and AIS and MIA in combination (1955 mm^3 ± 1576 [95% CI: 636, 3273]). Solid mass similarly differed between LPA and AIS and MIA (P = .042) in combination but not between INV and LPA.

The interobserver agreement was excellent for automated measures between the thoracic radiologist and radiology resident, ranging from 0.986 to 0.996 (Table 2). The agreement between the radiology resident and the medical student for automated measurement were also excellent, in the 0.991–9.997 range (Table 2).

Qualitative features are summarized in Figure 3. There was no association between pathologic subtype and shape, presence of pseudocavitation, internal reticulation, appearance of nodule margins, and central location ($P > .05$). A significant association between the pathologic subtype and the presence of a pleural tag was identified ($\chi^2 = 6.813$, $df = 2$, P = .041) (Fig 3).

When we used multivariate analysis to discriminate three different outcomes of INV, LPA, and AIS/MIA, the multinomial regression model based on visually evaluated morphologic variables had an overall accuracy of 56.1% (Table 3). In distinction, a model based on the combination of two quantitative variables using total volume and percentage solid volume had superior accuracy (overall, 73.2% correct) and provided a superior fit to the measurements (Table 3). Similar results were obtained when mass measures were used instead of volumes (Table 3). In a regression model with AIS/MIA as the reference category, the odds ratio for percentage solid volume was 1.4 and that for percentage solid by mass was 1.3. Thus, for each 1% increase in the solid fraction, an increase of about 40% in the odds of an INV versus an AIS/MIA outcome is expected.

Figure 2

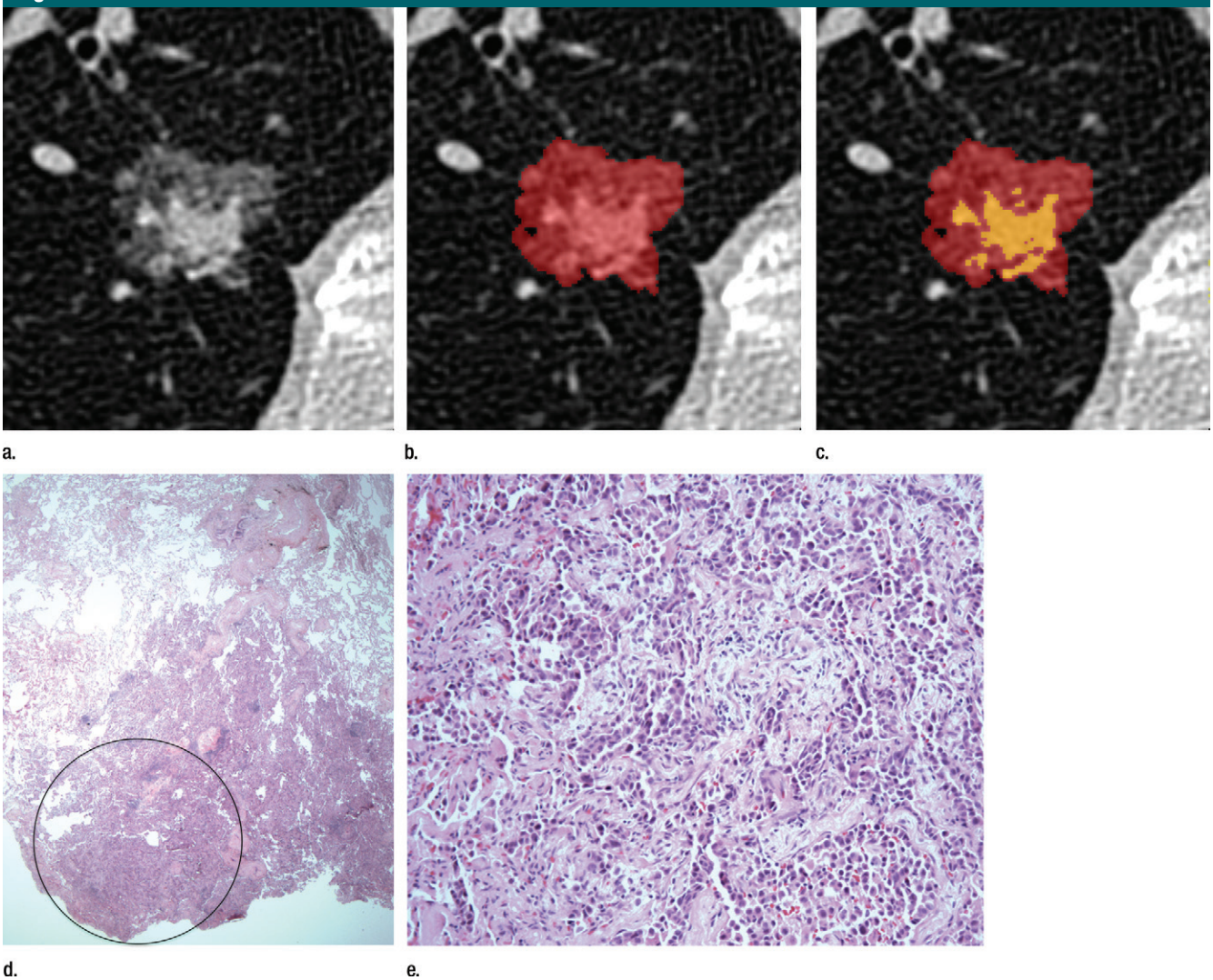

Figure 2: Images show quantitative evaluation of LPA in a 63-year-old woman. **(a)** Representative axial CT image of the tumor and **(b, c)** images with overlays of (**b**) the entire nodule and (**c**) solid areas of the nodule. **(d)** Staining showed tumor with lepidic (50%), acinar (10%), and papillary (40%) (circle) portions. (Hematoxylin-eosin stain; original magnification, ×20.) **(e)** At greater magnification, complex papillary structures filling alveolar spaces with central fibrovascular cores lined by cuboidal tumor cells are seen. (Hematoxylin-eosin stain; original magnification, ×200.)

Discussion

In this investigation, the automated analysis discriminated three cohorts of IASLC/ATS/ERS-classified lesions, grouped according to their differing 5-year disease-free patient survival rates (23,24), with accuracies of 73.2% for volumetric and 75.6% for mass measures. In addition, we have confirmed a high interreader agreement for an automated method for segmenting the solid from the ground-glass portions in a subsolid nodule. In contrast, morphologic features did not discriminate as well.

The multidisciplinary IASLC/ATS/ERS classification system (16) was issued in 2011 in response to the need to better classify lesions and differentiate patients with varying survivals (23,24). AIS comprises only lepidic noninvasive growth. MIA and LPA are also predominantly lepidic but also have invasive foci, the largest of which is 5 mm for MIA and larger than 5 mm for LPA (16). AIS, MIA, and LPA have 5-year disease-free survival rates of 100%, near 100%, and 90%, respectively (16,24). The 5-year disease-free survival rates of acinar- and papillary-predominant forms are reported to be 84% and 83%, while those of micropapillary- and solid-predominant adenocarcinomas have been reported to be 67% and 70%, respectively (16).

Subsolid nodules are associated with lung adenocarcinoma. Imaging features and linear dimensions of subsolid

Table 1

Differentiation of Pathologic Types of Adenocarcinomas

Measurement	AIS/MIA (n = 8)	LPA (n = 12)	INV (n = 21)	P Value for INV vs LPA*	P Value for LPA vs AIS/MIA*
Total volume (mm^3)	1955 ± 1576 (636, 3273)	4171 ± 3798 (1822, 6521)	3558 ± 3681 (1883, 5234)	NS	NS
Total solid volume (mm^3)	188 ± 255 (0, 401)	622 ± 600 (241, 1004)	1627 ± 2353 (556, 2698)	NS	.041
Percentage solid volume	8.2 ± 6.5 (2.7, 13.7)	14.5 ± 6.6 (10.3,18.7)	35.4 ± 20.2 (26.2,44.5)	.002	.051 (Trend)
Total mass (mg)	1025 ± 889 (282, 1768)	2442 ± 2139 (1083, 3801)	2717 ± 3106 (1303, 4131)	NS	NS
Solid mass (mg)	182 ± 248 (0, 389)	605 ± 590 (230, 979)	1654 ± 2431 (548, 2760)	NS	.042
Percentage solid mass	14.2 ± 10.6 (5.4, 23.1)	23.0 ± 8.8 (17.4, 28.6)	46.6 ± 21.2 (37.0, 56.3)	.001	NS

Note.—Data are means ± standard deviations, with 95% confidence intervals (CIs) in parentheses.

* NS = not significant.

Table 2

Intraclass Correlation Coefficients for Automated Nodule Measurements for Readers A and B

Measurement	Reader A	Reader B
Total volume	0.995 (0.990, 0.997)	0.991 (0.941, 0.998)
Solid volume	0.996 (0.991, 0.998)	0.996 (0.988, 0.998)
Percentage solid volume	0.986 (0.954, 0.996)	0.996 (0.965, 0.999)
Total mass	0.994 (0.990, 0.996)	0.993 (0.966, 0.998)
Solid mass	0.996 (0.991, 0.998)	0.996 (0.988, 0.998)
Percentage solid mass	0.989 (0.968, 0.997)	0.997 (0.975, 0.999)

Note.—Reader A was a thoracic radiologist and radiology resident; reader B was a resident and medical student. Data in parentheses are 95% CIs.

nodules were previously compared with pathologic findings categorized according to the Noguchi classification (17,25), with recent attention to the IASLC-classified tumors (19). Correlation of solid regions at CT with collapse, fibrosis, and invasion (11,26,27) and of the proportion of soft tissue at CT with invasive pathologic findings demonstrates the importance of estimating the soft-tissue areas in subsolid nodules. Nodules with larger solid components are associated with a higher likelihood of developing nodal metastases (1,28).

Quantitative assessment of the subsolid nodule has focused on the volume of the entire nodule and, more recently, of the solid region, primarily using visual assessment, manually measured linear dimensions, and, to a lesser degree, 3D methods (4,7,9,13,14,25,28–34). In patients with ground-glass nodules at lung cancer screening, de Hoop et al reported intra- and interobserver coefficients of variation of 15% and 18% for volumes derived from manually acquired linear two-dimensional measures to be greater than those for manually segmented 3D mass (9%) or volumes (9,14). Visual assessment, even by expert thoracic radiologists, had only moderate agreement when determining nodule attenuation, and identifying the presence of or amount of any solid component was the major cause of variation (35). Additionally, agreement between an experienced thoracic radiologist and one of less experience was only fair (κ = 0.309) when estimating the area ratio of ground-glass opacity in a nodule (32). Our excellent agreement supports the use of automated methods to minimize reader variation.

AIS/MIA in our study had only 8.2% ± 6.5 solid attenuation, correlating with prior reports of AIS and MIA as predominantly ground-glass nodules (16). The CT appearance of LPA and MIA have been less studied, although they are likely part-solid in attenuation (36,37). Our data support the positive association between the percentage of soft tissue at CT and invasive histopathologic features, with LPA having a mean percentage solid volume of 14.5%, which was significantly smaller than the 35.4% for INV. In contrast, total volume or total mass alone did not discriminate AIS/MIA, LPA, and INV, in support of the need to segment the solid from the ground-glass component within a subsolid nodule.

Our investigation had a number of limitations. We did not evaluate lung cancers other than adenocarcinoma. However, adenocarcinomas are the most common histopathologic subtype that often manifest as subsolid nodules and are challenging to characterize. We did not examine a reference group of clinically stable or benign ground-glass lesions. The ability to differentiate clinically stable nodules that are likely to represent indolent malignancy or preinvasive lesions from more aggressive malignancy would be of great benefit. An ability to differentiate preinvasive and minimally invasive lesions such as AIS and MIA from LPA and other invasive histologic findings would reduce overdiagnosis. We did not analyze nodule growth, which may prove a valuable indicator of aggressiveness, because thin-section images or prior chest CT studies were not available for a large majority of our adenocarcinomas.

Figure 3

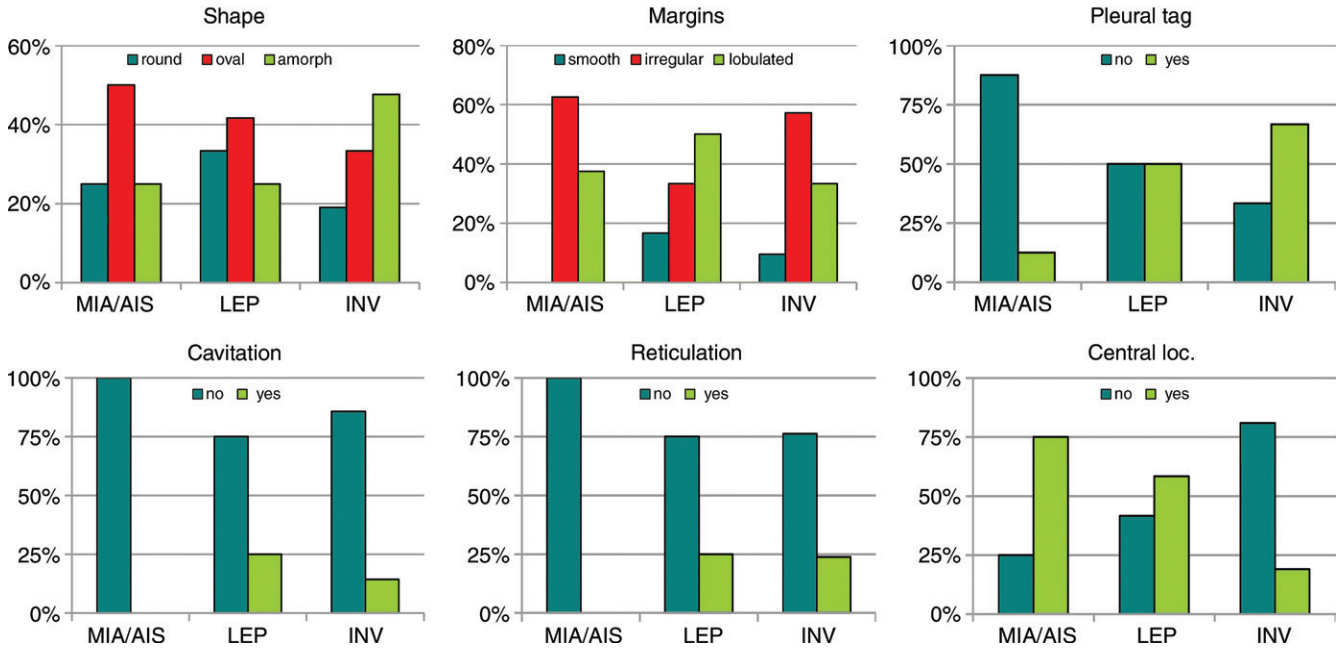

Figure 3: Graphs show distribution of morphologic nodule features. *Central loc.* = central location.

Table 3

Multinomial Regression Models for Differentiating Adenocarcinoma Subtypes

Parameter	Model A	Model B	Model C
No. of variables	6	2	2
Variables			
	Shape	Total volume	Total mass
	Pseudocavitation	Percentage solid volume	Percentage solid mass
	Internal reticulation		
	Margins		
	Location		
	Pleural tag		
Model-fitting information			
AIC	74.1	62.9	62.1
χ^2 Likelihood ratio test	22.1	32.8	33.6
P value	.076	<.001	<.001
R^2 value	0.479	0.632	0.643
Percentage correct			
AIS/MIA	62.1	75.0	62.5
LPA	41.7	50.0	58.3
INV	66.7	85.7	90.5
Overall	58.5	73.2	75.6

Note.—AIC = Akaike information criterion.

This investigation was a preliminary evaluation of an automated method for differentiating IASLC/ATS/ERS entities. A number of patients in the lung cancer database lacked thin-section imaging data owing to the protocols used in our department. The small number of AIS and MIA neoplasms in our current cohort probably relates to their lower likelihood of being resected, given their small size and less-aggressive imaging features. We did not visually assess nodule density, which has been shown to have large interobserver variation (35). Excellent correlation between the radiology resident and the expert radiologist showed that the automated technique was applicable to varying levels of experience and supported the role of subsolid nodule evaluation in clinical practice. Another limitation was the use of one site, with CT scanners from the same vendor. Finally, our method was not fully automated or commercially available, entailing several minutes. Our model included CT quantitative measures and did not include patient risk factors, and these probably influenced the clinical decision to resect these lesions. Regardless, the information brings to light the value of quantitative parameters for potentially discriminating lesions with varying prognoses. We did not analyze quantitative image texture and morphologic features, even though they may prove to be differentiators (38). We also did not correlate our measures with the molecular genetics of the adenocarcinomas.

In conclusion, a computer-assisted method can be used to derive reliable quantitative measures that distinguish varying histopathologic subtypes of adenocarcinoma with associated prognostic values. Precise computer-assisted measurement of the solid component volume and fraction can discriminate among IASLC/ATS/ERS subtypes of lung adenocarcinoma and therefore may potentially be used to accurately and noninvasively differentiate adenocarcinoma subtypes.

Acknowledgment: The authors acknowledge the assistance of Nicole Wake, MS, in data collection.

Disclosures of Conflicts of Interest: J.P.K. Activities related to the present article: none to disclose. Activities not related to the present article: is on the speakers bureau of Siemens. Other relationships: none to disclose. **J.S.** Activities related to the present article: none to disclose. Activities not related to the present article: is an employee of and has equity in Foundation Medicine; is a consultant for Pfizer and Daiichi-Sankyo; is on the speakers bureaus of Pfizer and Genentech. Other relationships: none to disclose. **O.I.** disclosed no relevant relationships. **J.G.E.** disclosed no relevant relationships. **J.L.** disclosed no relevant relationships. **H.P.** disclosed no relevant relationships. **D.P.N.** Activities related to the present article: none to disclose. Activities not related to the present article: is a consultant for Vida Diagnostics; is on the speakers bureau of Siemens; has received money for travel expenses from Vida Diagnostics and Siemens. Other relationships: none to disclose. **B.C.** disclosed no relevant relationships. **E.B.T.** disclosed no relevant relationships. **C.W.K.** disclosed no relevant relationships. **A.M.** disclosed no relevant relationships. **H.R.** disclosed no relevant relationships.

References

1. Aoki T, Tomoda Y, Watanabe H, et al. Peripheral lung adenocarcinoma: correlation of thin-section CT findings with histologic prognostic factors and survival. Radiology 2001; 220(3):803–809.
2. Tsutani Y, Miyata Y, Nakayama H, et al. Prognostic significance of using solid versus whole tumor size on high-resolution computed tomography for predicting pathologic malignant grade of tumors in clinical stage IA lung adenocarcinoma: a multicenter study. J Thorac Cardiovasc Surg 2012;143(3):607–612.
3. Okada M, Nishio W, Sakamoto T, et al. Correlation between computed tomographic findings, bronchioloalveolar carcinoma component, and biologic behavior of small-sized lung adenocarcinomas. J Thorac Cardiovasc Surg 2004;127(3):857–861.
4. Kakinuma R, Kodama K, Yamada K, et al. Performance evaluation of 4 measuring methods of ground-glass opacities for predicting the 5-year relapse-free survival of patients with peripheral nonsmall cell lung cancer: a multicenter study. J Comput Assist Tomogr 2008;32(5):792–798.
5. Yankelevitz DF, Reeves AP, Kostis WJ, Zhao B, Henschke CI. Small pulmonary nodules: volumetrically determined growth rates based on CT evaluation. Radiology 2000; 217(1):251–256.
6. Goo JM, Tongdee T, Tongdee R, Yeo K, Hildebolt CF, Bae KT. Volumetric measurement of synthetic lung nodules with multidetector row CT: effect of various image reconstruction parameters and segmentation thresholds on measurement accuracy. Radiology 2005;235(3):850–856.
7. Sumikawa H, Johkoh T, Nagareda T, et al. Pulmonary adenocarcinomas with ground-glass attenuation on thin-section CT: quantification by three-dimensional image analyzing method. Eur J Radiol 2008;65(1):104–111.
8. Zhang L, Yankelevitz DF, Carter D, Henschke CI, Yip R, Reeves AP. Internal growth of nonsolid lung nodules: radiologic-pathologic correlation. Radiology 2012;263(1): 279–286.
9. de Hoop B, Gietema H, van de Vorst S, Murphy K, van Klaveren RJ, Prokop M. Pulmonary ground-glass nodules: increase in mass as an early indicator of growth. Radiology 2010;255(1):199–206.
10. Scholten ET, Jacobs C, van Ginneken B, et al. Computer-aided segmentation and volumetry of artificial ground-glass nodules at chest CT. AJR Am J Roentgenol 2013; 201(2):295–300.
11. Aoki T, Nakata H, Watanabe H, et al. Evolution of peripheral lung adenocarcinomas: CT findings correlated with histology and tumor doubling time. AJR Am J Roentgenol 2000;174(3):763–768.
12. Suzuki K, Yokose T, Yoshida J, et al. Prognostic significance of the size of central fibrosis in peripheral adenocarcinoma of the lung. Ann Thorac Surg 2000;69(3):893–897.
13. Suzuki K, Kusumoto M, Watanabe S, Tsuchiya R, Asamura H. Radiologic classification of small adenocarcinoma of the lung: radiologic-pathologic correlation and its prognostic impact. Ann Thorac Surg 2006;81(2): 413–419.
14. Kim HY, Shim YM, Lee KS, Han J, Yi CA, Kim YK. Persistent pulmonary nodular ground-glass opacity at thin-section CT: histopathologic comparisons. Radiology 2007; 245(1):267–275.
15. Saito H, Yamada K, Hamanaka N, et al. Initial findings and progression of lung adenocarcinoma on serial computed tomography scans. J Comput Assist Tomogr 2009; 33(1):42–48.
16. Travis WD, Brambilla E, Noguchi M, et al. International Association for the Study of Lung Cancer/American Thoracic Society/European Respiratory Society international multidisciplinary classification of lung adenocarcinoma. J Thorac Oncol 2011;6(2):244–285.
17. Noguchi M, Morikawa A, Kawasaki M, et al. Small adenocarcinoma of the lung: histologic characteristics and prognosis. Cancer 1995;75(12):2844–2852.
18. Travis WD. Pathology of lung cancer. Clin Chest Med 2011;32(4):669–692.
19. Lim HJ, Ahn S, Lee KS, et al. Persistent pure ground-glass opacity lung nodules ≥ 10 mm in diameter at CT scan: histopathologic comparisons and prognostic implications. Chest 2013;144(4):1291–1299.
20. Hansell DM, Bankier AA, MacMahon H, McLoud TC, Müller NL, Remy J. Fleischner Society: glossary of terms for thoracic imaging. Radiology 2008;246(3):697–722.
21. Rusinek H, Naidich DP, McGuinness G, et al. Pulmonary nodule detection: low-dose versus conventional CT. Radiology 1998;209(1): 243–249.
22. Ko JP, Berman EJ, Kaur M, et al. Pulmonary nodules: growth rate assessment in patients by using serial CT and three-dimensional volumetry. Radiology 2012;262(2):662–671.
23. Yoshizawa A, Motoi N, Riely GJ, et al. Impact of proposed IASLC/ATS/ERS classification of lung adenocarcinoma: prognostic subgroups and implications for further revision of staging based on analysis of 514 stage I cases. Mod Pathol 2011;24(5): 653–664.
24. Yoshizawa A, Sumiyoshi S, Sonobe M, et al. Validation of the IASLC/ATS/ERS lung adenocarcinoma classification for prognosis and association with EGFR and KRAS gene mutations: analysis of 440 Japanese patients. J Thorac Oncol 2013;8(1):52–61.
25. Oda S, Awai K, Liu D, et al. Ground-glass opacities on thin-section helical CT: differentiation between bronchioloalveolar carcinoma and atypical adenomatous hyperplasia. AJR Am J Roentgenol 2008;190(5):1363–1368.
26. Aoki T, Hanamiya M, Uramoto H, Hisaoka M, Yamashita Y, Korogi Y. Adenocarcinomas with predominant ground-glass opacity: correlation of morphology and molecular biomarkers. Radiology 2012;264(2):590–596.

27. Takashima S, Maruyama Y, Hasegawa M, et al. Prognostic significance of high-resolution CT findings in small peripheral adenocarcinoma of the lung: a retrospective study on 64 patients. Lung Cancer 2002;36(3):289–295.

28. Yanagawa M, Tanaka Y, Kusumoto M, et al. Automated assessment of malignant degree of small peripheral adenocarcinomas using volumetric CT data: correlation with pathologic prognostic factors. Lung Cancer 2010;70(3):286–294.

29. Oda S, Awai K, Murao K, et al. Computer-aided volumetry of pulmonary nodules exhibiting ground-glass opacity at MDCT. AJR Am J Roentgenol 2010;194(2):398–406.

30. Park CM, Goo JM, Lee HJ, Kim KG, Kang MJ, Shin YH. Persistent pure ground-glass nodules in the lung: interscan variability of semiautomated volume and attenuation measurements. AJR Am J Roentgenol 2010; 195(6):W408–W414.

31. Oda S, Awai K, Murao K, et al. Volume-doubling time of pulmonary nodules with ground glass opacity at multidetector CT: assessment with computer-aided three-dimensional volumetry. Acad Radiol 2011;18(1):63–69.

32. Yanagawa M, Kuriyama K, Kunitomi Y, et al. One-dimensional quantitative evaluation of peripheral lung adenocarcinoma with or without ground-glass opacity on thin-section CT images using profile curves. Br J Radiol 2009;82(979):532–540.

33. Kim H, Park CM, Woo S, et al. Pure and part-solid pulmonary ground-glass nodules: measurement variability of volume and mass in nodules with a solid portion less than or equal to 5 mm. Radiology 2013;269(2):585–593.

34. Yanagawa M, Tanaka Y, Leung AN, et al. Prognostic importance of volumetric measurements in stage I lung adenocarcinoma. Radiology 2014;272(2):557–567.

35. van Riel SJ, Sánchez CI, Bankier AA, et al. Observer variability for classification of pulmonary nodules on low-dose CT images and its effect on nodule management. Radiology 2015;277(3):863–871.

36. Austin JH, Garg K, Aberle D, et al. Radiologic implications of the 2011 classification of adenocarcinoma of the lung. Radiology 2013; 266(1):62–71.

37. Ambrosini-Spaltro A, Ruiu A, Seebacher C, et al. Impact of the IASLC/ATS/ERS classification in pN0 pulmonary adenocarcinomas: a study with radiological-pathological comparisons and survival analyses. Pathol Res Pract 2014;210(1):40–46.

38. Chae HD, Park CM, Park SJ, Lee SM, Kim KG, Goo JM. Computerized texture analysis of persistent part-solid ground-glass nodules: differentiation of preinvasive lesions from invasive pulmonary adenocarcinomas. Radiology 2014;273(1):285–293.